

Cite as: Appl. Phys. Lett. **117**, 162102 (2020); doi: 10.1063/5.0023246 Submitted: 27 July 2020 · Accepted: 16 September 2020 · Published Online: 19 October 2020







Scott A. McClary, 1 (1) Mohammad M. Taheri, 2 (1) Daria D. Blach, 3 (1) Apurva A. Pradhan, 1 (1) Siming Li, 2 (1) Libai Huang, 3 (1) Jason B. Baxter, 2, a) (1) and Rakesh Agrawal 1, a) (1)

AFFILIATIONS

- ¹Davidson School of Chemical Engineering, Purdue University, 480 Stadium Mall Drive, West Lafayette, Indiana 47907, USA
- ²Department of Chemical and Biological Engineering, Drexel University, 3141 Chestnut Street, Philadelphia, Philadelphia 19104, USA

ABSTRACT

Enargite (ENG) Cu₃AsS₄ is a promising material for photovoltaic applications due to its constituent earth abundant elements of differing ionic radii, ideal predicted optoelectronic properties, and demonstrated use in a working thin-film solar cell. However, little is known about ENG's defect properties; such knowledge is necessary to assess its potential for future use in high-efficiency devices. One indicator of a material's quality is its photogenerated carrier lifetime, which can be related to its bulk defect properties. Here, we use a combination of time-resolved terahertz spectroscopy and time-resolved photoluminescence to assess carrier dynamics in ENG thin films processed from nanoparticle precursors. The Shockley–Read–Hall (SRH) lifetimes are on the multi-nanosecond scale, which exceed those reported in more mature systems and represent promising values for a candidate photovoltaic material. These results suggest that ENG is worthy of further research and development effort with an eye toward future photovoltaic applications.

Published under license by AIP Publishing. https://doi.org/10.1063/5.0023246

Thin-film photovoltaic (PV) devices have received intense research attention over the past few decades due to the potential of low-cost electricity production with minimal greenhouse gas emissions. PV modules incorporating CdTe and Cu(In,Ga)Se₂ (CIGSe) absorber layers have been commercialized, but their ultimate market penetration may be limited due to uncertainty regarding the long-term availability and price volatility of Te and In. 1,2 As a result, materials containing earth-abundant elements have been studied, with the most notable being Cu₂ZnSn(S_{1-x}Se_x)₄ (CZTSSe). Unfortunately, efficiencies of CZTSSe-based devices have stalled since IBM's record 12.6% solar cell was reported in late 2013, in part because Cu and Zn readily form antisite defects due to their similar ionic radii and charge states.⁵⁻⁸ The resulting disordered structure leads to band tailing and electrostatic potential fluctuations, which limit the open-circuit voltage and, hence, efficiency of PV devices. 9-11 Such intrinsic flaws may prove too challenging to overcome in a meaningful timeframe, and so alternative options must be explored.

Copper arsenic sulfide (Cu₃AsS₄) in the orthorhombic enargite (ENG) crustal structure is one promising alternative material for PV applications due to the crystal abundance of Cu, As, and S, as well as a low likelihood of cation disorder because of the differing ionic radii

and charge states of its constituent elements. Basic optoelectronic properties of ENG were measured several decades ago, 12 and more recent computational studies revealed ideal optoelectronic properties and the potential for high efficiencies in thin-film ENG PV devices. $^{13-15}$ In addition, solution-based synthetic protocols for various Cu–As–S nanoparticles (NPs) and thin films have recently been developed. $^{16-20}$ Using Cu₃AsS₄ NPs as a precursor, our group fabricated the first PV devices with a large-grained ENG absorber layer, but the power conversion efficiencies were modest. 21 Several factors, including poor band alignment with n-type CdS 22 and film porosity, likely contributed to low efficiencies and are the subject of parallel research effort.

As is the case with any emerging material, it is imperative to rapidly gauge ENG's potential to determine if extensive research and development efforts are warranted or if intrinsically limiting issues (e.g., large defect populations, band tailing, etc.) will hinder its long-term development. One indicator of a material's quality is the photogenerated carrier lifetime, which is strongly correlated with defect properties. High populations of mid-gap defects can result in high recombination rates for excess carriers, which reduce the average carrier lifetime and, hence, PV device performance. In this study, we use

³Department of Chemistry, Purdue University, 560 Oval Drive, West Lafayette, Indiana 47907, USA

^{a)}Authors to whom correspondence should be addressed: jbaxter@drexel.edu and agrawalr@purdue.edu

time-resolved terahertz spectroscopy (TRTS)^{23–25} and time-resolved photoluminescence (TRPL)^{26–29} to study photogenerated carrier dynamics in ENG thin films grown on a variety of substrates. In all cases, the Shockley–Read–Hall (SRH) recombination lifetime is on the order of nanoseconds, suggesting that carrier dynamics in ENG are favorable for PV applications.

ENG thin films were fabricated using our previously developed methods;²¹ full details are provided in the supplementary material. Briefly, Cu₃AsS₄ NPs in the luzonite phase were synthesized^{16,18} and coated onto four substrates: quartz, soda-lime glass (SLG), molybdenum-coated soda-lime glass (Mo-SLG), and molybdenum-coated borosilicate glass (Mo-BSG). Quartz facilitated the study of ENG films without extrinsic alkali dopants, while the other three were chosen due to their higher alkali content and use in established CIGSe and CZTSSe PV device architectures.^{4,30–32} Samples were vacuum sealed in glass ampoules with As₂S₅ powder and annealed for 30 min at 425 °C. The treatments yielded thin films with a bilayer structure: relatively dense grains sit on top of a small "fine-grain" layer commonly reported in other NP-derived systems (Fig. S1, supplementary material).

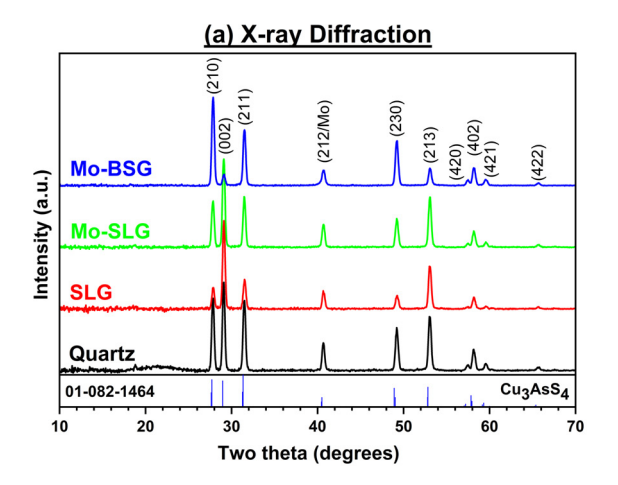
Grazing incidence x-ray diffraction (GIXRD, Fig. 1(a), $\lambda = 1.5406 \text{ Å}$) confirms that ENG is the only crystalline phase in all four samples. Each pattern has sharp peaks (signifying large crystalline domains) that align with an ENG single crystal standard.33 In the quartz spectrum, a broad stretch centered near 22° 2θ is attributable to the amorphous substrate. In the spectra of Mo-containing samples, the peak near $40^{\circ} 2\theta$ results from an overlap of diffraction peaks from the ENG (212) plane and the (110)oriented Mo substrate. Some evidence of crystallographic texture is present, as the SLG and Mo-SLG samples display exaggerated (002) peaks, while the Mo-BSG sample displays a diminished (002) peak. The factors controlling preferred orientation of ENG are not clear at this point, but it is noteworthy that alkali metal (e.g., sodium) doping has been linked to the growth of textured films of CIGSe and CZTSSe. 31,34-36 Computational work suggests that ENG has an anisotropic effective hole mass, 15 suggesting that films

with variable crystallographic texturing may differ in their carrier transport properties.

Raman spectroscopy [Fig. 1(b), $\lambda = 633$ nm] further confirms the formation of ENG in all four samples. Each spectrum displays a dominant transverse optical (TO) mode at 340 cm⁻¹, a longitudinal optical (LO) mode around $380\,\mathrm{cm}^{-1}$, and another mode around $270\,\mathrm{cm}^{-1}$, in agreement with a mineral reference and previous reports.3 Additionally, each spectrum has peaks near 494 cm⁻¹, 565 cm⁻¹, and 360 cm⁻¹ that correspond to an amorphous secondary phase originating partially from carbonaceous ligands on the NP precursors.²¹ X-ray fluorescence (XRF) measurements (Table SI, supplementary material) indicate that the as-treated samples were arsenic-rich, likely due to condensation of excess As-S vapors on the films' surfaces. Nearstoichiometry was restored after a 1 min immersion in (NH₄)₂S solution, which is known to dissolve As-S compounds.^{39–41} This etch caused films on quartz to delaminate and flake off almost completely, and so carrier dynamics measurements were conducted on unetched quartz samples. The degree of delamination was much lower on SLG and nonexistent on Mo-SLG and Mo-BSG.

Transmission-mode TRTS was used to probe carrier dynamics in ENG thin films fabricated on quartz [Fig. 2(a)]. Samples were photo-excited by $\sim\!\!50$ fs laser pulses of tunable wavelength and intensity and then probed with a terahertz pulse as a function of pump—probe delay time to obtain insight into transient photoconductivity.^23-25 TRPL [Fig. 2(b)] was also used to probe carrier dynamics in ENG thin films on quartz, but by means of transient photoluminescence. Samples were photoexcited by 447 nm $\sim\!\!50$ ps laser pulses, and the PL resulting from radiative recombination was monitored. For both TRTS and TRPL, incident photon densities corresponding to high injection levels $(\sim\!10^{18}\!-\!10^{19}\,\mathrm{cm}^{-3}$, vs a hole concentration of $\sim\!10^{16}\,\mathrm{cm}^{-3}$ determined from Hall effect measurements) were intentionally chosen to quantify radiative and Auger recombination rate constants.

The TRTS response shows that photoconductivity persists beyond the ~ 1.4 ns detection range, suggesting that carrier lifetimes in ENG films are at least on the nanosecond scale. The TRPL response decays significantly faster than the TRTS response, with less than 5%



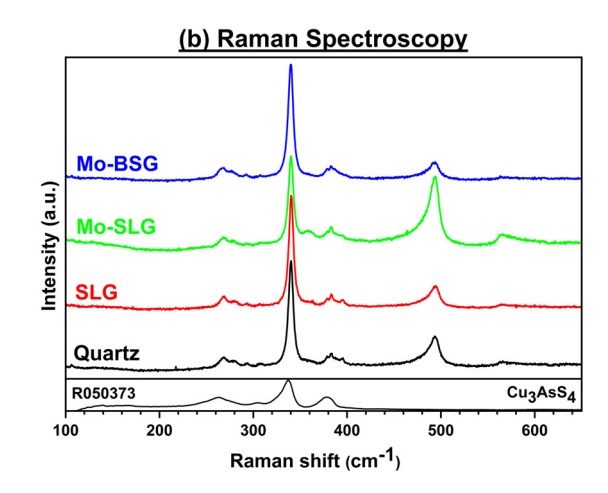
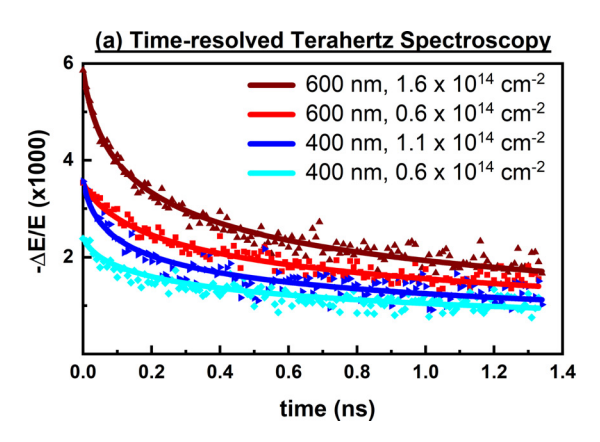


FIG. 1. (a) GIXRD and (b) Raman spectra of enargite thin films fabricated on various substrates. The GIXRD peaks match with JCPDS reference 01-082-1464, and the Raman peaks align well with RRUFF reference R050373, with additional Raman peaks attributed to a secondary phase originating in part from carbonaceous ligands on the nanoparticle precursors.



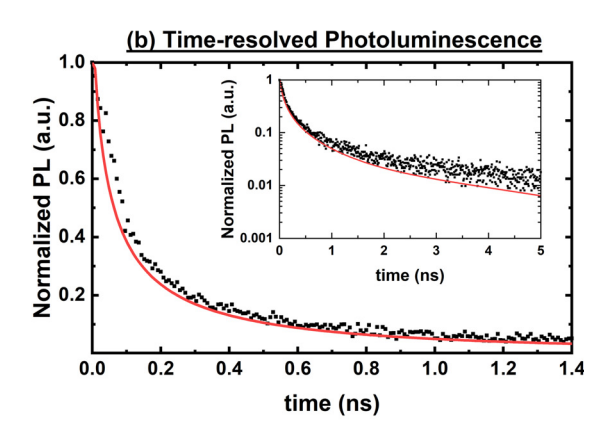


FIG. 2. (a) Transmission-TRTS dynamics as a function of pump wavelength and incident photon flux for an ENG film on quartz. The change in the terahertz electric field (ΔE) is normalized by the magnitude of a reference pulse (E). (b) TRPL dynamics at a wavelength of 447 nm and an incident photon flux of 2.4 × 10¹⁴ cm⁻² (inset: extended TRPL data on the logarithmic scale). The solid lines are the global fit of Eq. (1) simultaneously to the TRPL and TRTS experimental data.

of the original signal remaining after 1 ns. The apparent discrepancy arises because TRTS and TRPL signals are proportional to different quantities—TRTS is sensitive to the sum of electrons and holes (since each contributes independently to conductivity), while TRPL is sensitive to the product of electrons and holes at the high injection levels used here (since one of each is required for PL). The electron-hole product decreases quickly as carriers diffuse to relieve concentration gradients arising from the initial Beer's Law generation profile, resulting in a decrease in the signal even without recombination. TRPL signals, therefore, decay inherently faster than TRTS signals, and careful modeling is required to extract carrier lifetimes.

The time-dependent continuity equation [Eq. (1)] was used to model the photoexcited carrier dynamics, with recombination rate equations in the high injection limit,

$$\frac{\partial n}{\partial t} = D \frac{\partial^2 n}{\partial x^2} - k_{SRH} n - k_{rad} n^2 - k_{Aug} n^3.$$
 (1)

In Eq. (1), n is the excess carrier density upon photoexcitation and k_{SRH} , k_{rad} , and k_{Aug} are the SRH, radiative, and Auger recombination coefficients, respectively. Due to high injection levels, we assumed that p(x,t) = n(x,t) (where p and n are the hole and electron concentrations) and that carriers move by ambipolar diffusion with coefficient D, with no extended electric fields.

The TRTS and TRPL signals depicted in Fig. 2 were simultaneously modeled using Eq. (1) to extract rate constants and the ambipolar diffusion coefficient. The TRTS signal is proportional to $\int n(x,t)dx$, and the TRPL signal is proportional to $\int n(x,t)^2 dx$. The initial distribution of carriers was modeled using Beer's Law [Eq. (2)] with absorption coefficients (α) at 400, 447, and 600 nm estimated to be $1.15 \times 10^5 \,\mathrm{cm}^{-1}$, $1.3 \times 10^5 \,\mathrm{cm}^{-1}$, and $6.2 \times 10^4 \,\mathrm{cm}^{-1}$, respectively. Front surface recombination velocity (SRV_{front}) was considered [Eq. (3)], but back surface recombination was ignored [Eq. (4)] because the optical penetration depths $(1/\alpha)$ for wavelengths of 400, 447, and 600 nm (87, 77, and 161 nm) and the diffusion length (~270 nm, see the supplementary material) are much smaller than the film thickness ($\sim 1 \,\mu\text{m}$),

$$n(x, t = 0) = n_0 \exp(-\alpha x), \tag{2}$$

$$\frac{\partial n(x=0,t)}{\partial x} = \frac{SRV_{front}}{D}n(0,t),$$

$$\frac{\partial n(x=L_{film},t)}{\partial x} = 0.$$
(4)

$$\frac{\partial n(x = L_{film}, t)}{\partial x} = 0.$$
(4)

Table I shows the best fit parameters for two cases: one where Dis a free parameter and another where $D = 0.05 \,\mathrm{cm}^2 \,\mathrm{s}^{-1}$, corresponding to an ambipolar mobility of 2.0 cm² V⁻¹ s⁻¹ (further details are given in the supplementary material). Due to challenges in measuring D, a "reasonable-fit" range is also provided, resulting from a sensitivity analysis in which D was varied from $0-2 \text{ cm}^2 \text{ s}^{-1}$ (the details are provided in the supplementary material, Figs. S2-S4 and Tables SII-SIII). The small k_{SRH} values correspond to SRH lifetimes well beyond the temporal range of the THz spectroscopy stage (1.4 ns), indicating that SRH recombination proceeds on at least the nanosecond timescale in ENG films on quartz. Table I also shows that at these testing conditions, all four modes of recombination occur in appreciable quantities (see the supplementary material for calculation details). However, the relative contributions of radiative and Auger processes will decrease at lower injection levels more relevant to PV operation, whereas both SRH and surface recombination will still occur in appreciable amounts due to their linear scaling with carrier density. Regardless, the SRH lifetime is significantly longer than 1.4 ns, which exceeds the reported lifetimes (hundreds of ps to 1-2 ns) of materials in the well-established CZTSSe^{23,25} system. The lifetime also compares favorably with more recently explored materials—CuSbSe₂ films incorporated into a 4.7% efficient device exhibited a lifetime of 190 ps,²⁴ and Sb₂Se₃ films in an 8.2% efficient device possessed a lifetime of 1339 ps. 42 The lifetime >1.4 ns for ENG, thus, represents a promising initial benchmark for a candidate material.

To compare carrier dynamics in ENG films grown on quartz, SLG, Mo-SLG, and Mo-BSG substrates, TRTS was used in reflection geometry (Fig. 3) because of the small transmitted THz signals through the latter three materials. To verify the applicability of reflection measurements, data were collected in both transmission and reflection geometries on a quartz sample; the responses (Fig. S5 in the supplementary material) were similar in both modes. Furthermore, the SLG, Mo-SLG, and Mo-BSG samples were etched in (NH₄)₂S to remove excess surface residue; TRTS and TRPL measurements on

TABLE I. Best-fit values for variable D and fixed $D = 0.05 \, \mathrm{cm^2 \, s^{-1}}$, the reasonable-fit range for parameters in Eqs. (1)–(4) using TRTS and TRPL data from an ENG film fabricated on quartz, and the fraction of recombined carriers at a photon flux of $0.6 \times 10^{14} \, \mathrm{cm^{-2}}$, a wavelength of 400 nm, and a fixed k_{SRH} value of $10^8 \, \mathrm{s^{-1}}$. The fraction of radiative and Auger recombination will be significantly lower at PV-relevant intensities.

Parameter	Variable D	D = 0.05	Reasonable-fit range	Carrier fraction
k_{SRH} (s ⁻¹)	$\ll 6.5 \times 10^{8}$	$\ll 6.5 \times 10^{8}$	$\ll 6.5 \times 10^{8}$	22%
k_{rad} (cm ³ s ⁻¹)	4.6×10^{-10}	2.3×10^{-10}	$(1.5-7.0) \times 10^{-10}$	25%
k_{Aug} (cm ⁶ s ⁻¹)	4.1×10^{-28}	4.0×10^{-28}	$(3.5-5.9) \times 10^{-28}$	20%
SRV_{front} (cm s ⁻¹)	9.8×10^{3}	6.1×10^{3}	$(5.0-11) \times 10^3$	33%
$D \left(\text{cm}^2 \text{ s}^{-1} \right)$	0.54	0.05	0.03-0.8	

Mo-SLG samples suggest that this etch has a minimal effect on the overall carrier dynamics (Fig. S6 in the supplementary material). The photoconductivity decays more slowly in the SLG sample than in the quartz one, suggesting longer lifetimes for photogenerated carriers. Two differences between the films are that the SLG sample is more highly textured along the (002) plane and that alkali diffusion from the substrate may have occurred. Carrier lifetimes in both CIGSe and CZTSSe thin films have benefitted from increased texturing 31,35 and sodium incorporation; 43,44 similar mechanisms may affect ENG and will be investigated in a future study. The slower photoconductivity decay is consistent across wavelengths from 400–800 nm, covering both surface and bulk regimes (Fig. S7 in the supplementary material).

The TRTS data from the Mo-SLG and Mo-BSG samples are ill-suited for fitting to Eq. (1) because the large refractive index of Mo significantly reduces the signal-to-noise ratio of the reflected TRTS signal. To compare lifetimes across all four substrates, TRPL data were fit using Eq. (1) to extract rate constants (Fig. S9, Table SIV in the supplementary material). The extracted SRH rate constants demonstrate that the ENG film on quartz has the lowest SRH lifetime (\sim 3 ns), consistent with the TRTS data. The effect of the substrate on recombination coefficients requires further study; however, the fact that the SRH lifetime is on the order of nanoseconds for all substrates is promising for the future of ENG as a photovoltaic material.

We stress that our carrier dynamics results are preliminary. Developments in ENG film synthesis will facilitate additional

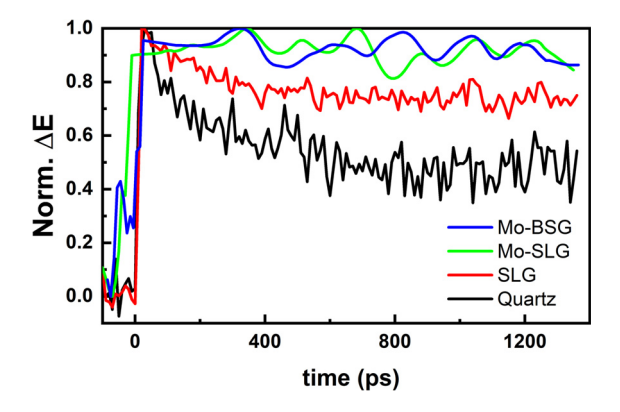


FIG. 3. Normalized reflection-TRTS dynamics at incident photon fluxes of $5.9 \times 10^{13} \, \mathrm{cm^{-2}}$ (for quartz and SLG) or $2.3 \times 10^{14} \, \mathrm{cm^{-2}}$ (for Mo-SLG and Mo-BSG) for a pump wavelength of 400 nm. The kinetics for the Mo-SLG and Mo-BSG samples were smoothed in OriginPro using the Lowess method with a 0.15 span; raw data are shown in the supplementary material (Fig. S8).

measurements and modeling using TRTS and TRPL. The TRPL spectra, in particular, will benefit from higher signal resolution and additional temperature-, intensity-, and voltage-dependent measurements²⁷ on thin films and completed devices to determine the origins of the substrate-dependent decays seen in this work. The time-resolved experiments will be supplemented by electronic and materials characterization techniques aimed at determining the distribution of defects throughout the films and their impact on carrier lifetimes.

In summary, we have characterized the carrier dynamics in enargite Cu_3AsS_4 thin films with a combination of time-resolved terahertz and time-resolved photoluminescence spectroscopies. In ENG thin films, Shockley–Read–Hall recombination occurs on the timescale of nanoseconds or longer, corresponding to lifetimes that exceed those in the well-studied CZTSSe system and are well comparable to those in other emerging materials such as Sb_2Se_3 . The carrier dynamics will likely improve as further advances are made in ENG fabrication procedures, resulting in high-quality thin films for device applications. These exciting results motivate further research into enargite Cu_3AsS_4 as a material for earth-abundant photovoltaic devices.

See the supplementary material for further details regarding experimental procedures, supplemental characterization of enargite thin films, calculation details pertaining to mobility and relative rates of recombination mechanisms, sensitivity analysis of the diffusion and recombination coefficients, and additional plots related to TRTS and TRPL.

This work was supported by the National Science Foundation under the DMREF Program (Nos. DMR-1534691 and DMR-1507988), the Research Traineeship Program (Award No. NRT-1735282), and the Division of Chemistry (No. CHE-1708991). The TRPL measurements were supported by the U.S. Department of Energy, Office of Basic Energy Sciences through Award No. DE-SC0016356. S.A.M. acknowledges Purdue University for a Bilsland Dissertation Fellowship. D.D.B. acknowledges Purdue University for a Frederick N. Andrews Fellowship. The authors thank Xianyi Hu, Essam AlRuqobah, and Joseph Andler for fabricating Mocoated substrates and Yining Feng, Kyle Weideman, and Professor Luna Lu for assistance with Hall effect measurements. The authors declare no competing financial interests.

DATA AVAILABILITY

The data that support the findings of this study are openly available in DEEDS at https://datacenterhub.org/groups/dmref1534691, Ref. 46.

REFERENCES

- ¹C. Wadia, A. P. Alivisatos, and D. M. Kammen, Environ. Sci. Technol. 43, 2072 (2009).
- (2009). ²C. Candelise, M. Winskel, and R. Gross, Prog. Photovoltaics Res. Appl. **20**, 816 (2012).
- ³Copper Zinc Tin Sulfide-Based Thin Film Solar Cells, 1st ed., edited by K. Ito (John Wiley & Sons, Ltd., 2015).
- ⁴W. Wang, M. T. Winkler, O. Gunawan, T. Gokmen, T. K. Todorov, Y. Zhu, and D. B. Mitzi, Adv. Energy Mater. 4, 1301465 (2014).
- ⁵S. Chen, X. G. Gong, A. Walsh, and S. H. Wei, Appl. Phys. Lett. **96**, 021902 (2010).
- ⁶S. Schorr, Sol. Energy Mater. Sol. Cells **95**, 1482 (2011).
- ⁷S. Chen, A. Walsh, X. G. Gong, and S. H. Wei, Adv. Mater. **25**, 1522 (2013).
- ⁸N. A. Kattan, I. J. Griffiths, D. Cherns, and D. J. Fermín, Nanoscale **8**, 14369 (2016).
- ⁹T. Gokmen, O. Gunawan, T. K. Todorov, and D. B. Mitzi, Appl. Phys. Lett. 103, 103506 (2013).
- ¹⁰C. J. Hages, N. J. Carter, and R. Agrawal, J. Appl. Phys. 119, 014505 (2016).
- ¹¹S. Giraldo, Z. Jehl, M. Placidi, V. Izquierdo-Roca, A. Pérez-Rodríguez, and E. Saucedo, Adv. Mater. 31, 1806692 (2019).
- ¹²T. Pauporté and D. Lincot, Adv. Mater. Opt. Electron. 5, 289 (1995).
- ¹³L. Yu, R. S. Kokenyesi, D. A. Keszler, and A. Zunger, Adv. Energy Mater. 3, 43 (2013).
- ¹⁴T. Shi, W.-J. Yin, M. Al-Jassim, and Y. Yan, Appl. Phys. Lett. **103**, 152105 (2013).
- ¹⁵S. K. Wallace, K. L. Svane, W. P. Huhn, T. Zhu, D. B. Mitzi, V. Blum, and A. Walsh, Sustainable Energy Fuels 1, 1339 (2017).
- ¹⁶R. B. Balow, E. J. Sheets, M. M. Abu-Omar, and R. Agrawal, Chem. Mater. 27, 2290 (2015).
- ¹⁷A. Das, A. Shamirian, and P. T. Snee, Chem. Mater. **28**, 4058 (2016).
- ¹⁸R. B. Balow, C. K. Miskin, M. M. Abu-Omar, and R. Agrawal, Chem. Mater. 29, 573 (2017).
- ¹⁹S. A. McClary, R. B. Balow, and R. Agrawal, J. Mater. Chem. C **6**, 10538 (2018).
- ²⁰S. A. McClary and R. Agrawal, MRS Commun. **10**, 188 (2020).
- ²¹S. A. McClary, J. Andler, C. A. Handwerker, and R. Agrawal, J. Mater. Chem. C 5, 6913 (2017).
- ²²S. K. Wallace, K. T. Butler, Y. Hinuma, and A. Walsh, J. Appl. Phys. 125, 055703 (2019).
- ²³G. W. Guglietta, K. R. Choudhury, J. V. Caspar, and J. B. Baxter, Appl. Phys. Lett. **104**, 253901 (2014).
- ²⁴A. W. Welch, L. L. Baranowski, H. Peng, H. Hempel, R. Eichberger, T. Unold, S. Lany, C. Wolden, and A. Zakutayev, Adv. Energy Mater. 7, 1601935 (2017).

- ²⁵S. Li, M. A. Lloyd, H. Hempel, C. J. Hages, J. A. Márquez, T. Unold, R. Eichberger, B. E. McCandless, and J. B. Baxter, Phys. Rev. Appl. 11, 034005 (2019).
- ²⁶F. Staub, H. Hempel, J. C. Hebig, J. Mock, U. W. Paetzold, U. Rau, T. Unold, and T. Kirchartz, Phys. Rev. Appl. 6, 044017 (2016).
- ²⁷C. J. Hages, A. Redinger, S. Levcenko, H. Hempel, M. J. Koeper, R. Agrawal, D. Greiner, C. A. Kaufmann, and T. Unold, Adv. Energy Mater. 7, 1700167 (2017).
- 28T. Zhu, L. Yuan, Y. Zhao, M. Zhou, Y. Wan, J. Mei, and L. Huang, Sci. Adv. 4, eaao3104 (2018).
- ²⁹T. P. Weiss, B. Bissig, T. Feurer, R. Carron, S. Buecheler, and A. N. Tiwari, Sci. Rep. 9, 5385 (2019).
- ³⁰S. M. McLeod, C. J. Hages, N. J. Carter, and R. Agrawal, Prog. Photovoltaics Res. Appl. 23, 1550 (2015).
- ⁵¹C. J. Hages, M. J. Koeper, C. K. Miskin, K. W. Brew, and R. Agrawal, Chem. Mater. 28, 7703 (2016).
- 32T. Kato, J. Wu, Y. Hirai, H. Sugimoto, and V. Bermudez, IEEE J. Photovoltaics 9, 325 (2019).
- ³³J. A. Henao, G. Díaz de Delgado, J. M. Delgado, F. J. Castrillo, and O. Odreman, Mater. Res. Bull. 29, 1121 (1994).
- ³⁴J. R. Tuttle, M. Contreras, M. H. Bode, D. Niles, D. S. Albin, R. Matson, A. M. Gabor, A. Tennant, A. Duda, and R. Noufi, J. Appl. Phys. 77, 153 (1995).
- 35 M. A. Contreras, M. J. Romero, and R. Noufi, Thin Solid Films 511–512, 51 (2006).
- ³⁶W. M. Hlaing Oo, J. L. Johnson, A. Bhatia, E. A. Lund, M. M. Nowell, and M. A. Scarpulla, J. Electron. Mater. 40, 2214 (2011).
- ³⁷T. P. Mernagh and A. G. Trudu, Chem. Geol. **103**, 113 (1993).
- ³⁸J. Ásbjörnsson, G. H. Kelsall, R. A. D. Pattrick, D. J. Vaughan, P. L. Wincott, and G. A. Hope, J. Electrochem. Soc. 151, E250 (2004).
- ³⁹M. V. Kovalenko, M. I. Bodnarchuk, J. Zaumseil, J.-S. Lee, and D. V. Talapin, J. Am. Chem. Soc. **132**, 10085 (2010).
- ⁴⁰S. Yakunin, D. N. Dirin, L. Protesescu, M. Sytnyk, S. Tollabimazraehno, M. Humer, F. Hackl, T. Fromherz, M. I. Bodnarchuk, M. V. Kovalenko, and W. Heiss, ACS Nano 8, 12883 (2014).
- ⁴¹Z. Xia, J. Zhong, M. Leng, L. Hu, D.-J. J. Xue, B. Yang, Y. Zhou, X. Liu, S. Qin, Y.-B. B. Cheng, and J. Tang, Chem. Mater. 27, 8048 (2015).
- ⁴²X. Wen, C. Chen, S. Lu, K. Li, R. Kondrotas, Y. Zhao, W. Chen, L. Gao, C. Wang, J. Zhang, G. Niu, and J. Tang, Nat. Commun. 9, 2179 (2018).
- 43 U. Rau and H. W. Schock, *Sol. Cells*, 2nd ed. (Elsevier, 2013), pp. 261–304.
- 44Z. Tong, F. Liu, L. Jiang, and Y. Lai, Mater. Lett. 254, 50 (2019).
- 45 H. Hempel, T. Unold, and R. Eichberger, Opt. Express 25, 17227 (2017).
- 46S. A. McClary, Y. Yan, and R. Agrawal (2017). "Rapid design of earth abundant inorganic materials for future PVs," DEEDS, https://datacenterhub.org/groups/ dmref1534691